Thermally Activated Transient Dipoles and Rotational Dynamics of Hydrogen-Bonded and Charge-Transferred Diazabicyclo [2.2.2]octane Molecular Rotors

Xing Jiang,[†] Hai-Bao Duan,[*, ‡, †] Marcus Jellen,[†] Tim S. Chung,[†] Yong Liang,[§] and Miguel A. Garcia-Garibay[*,†]

[†]Department of Chemistry and Biochemistry, University of California, Los Angeles, California 90095, United States

[‡]School of Environmental Science, Nanjing Xiao Zhuang University, Nanjing, Jiangsu 211171, P.R. China

[§]State Key Laboratory of Coordination Chemistry, School of Chemistry and Chemical Engineering, Nanjing University, Nanjing, Jiangsu 210023, P.R. China

ABSTRACT: We present here dielectric properties and rotational dynamics of cocrystals formed with either triphenylacetic acid (cocrystal **I**) or 9,10-triptycene dicarboxylic acid (cocrystal **II**), as hydrogen bonding donors, and diazabicyclo[2.2.2]octane (DABCO) as a ditopic hydrogen bond acceptor. While cocrystal **I** forms discrete 2:1 complexes with one nitrogen of DABCO hydrogen bonded and the other fully protonated, cocrystal **II** consists of 1:1 complexes forming infinite 1-D hydrogen bonded chains capable of exhibiting thermally activated response in the form of a broad asymmetric peak at ca. 298 K that extends from ca. 200 K to 375 K in both the real and imaginary parts of its complex dielectric. The state of protonation in cocrystal **II** at 298 K and at 386 K was established by CPMAS ^{15}N NMR, which showed signals typical of a neutral hydrogen bonded complex. Taken together, these observations suggest a dielectric response that results from of a small population of transient dipoles thermally generated when acidic protons are transiently transferred to either side of the DABCO base. A potential order-disorder transition explored by taking advantage of the highly sensitive rotational dynamics of the DABCO group using line shape analysis of solid state spin echo ^{2}H NMR and ^{1}H T_1 spin lattice-relaxation showed no breaks in the Arrhenius plot or Kubo-Tomita ^{1}H T_1 fittings, indicating that there are no large changes in the structure. This was confirmed by VT single crystal X-ray diffraction analysis, which showed a fairly symmetric hydrogen bond in cocrystal **II,** suggesting that both nitrogen atoms may be able to adopt a protonated state.

INTRODUCTION

Hydrogen bond (H-bond) donors and acceptors and their proton transfer (H-transfer) derivatives are not only among the best understood and more versatile synthons in crystal engineering,[1] but structures with double donors and/or double acceptors provide interesting possibilities for the design of tailor-made dielectric materials.[2] In particular, a number of ferroelectric crystals involving dibasic 1,4-diazabicyclo[2.2.2]octane (dabco)[3] complexes with strong organic[4,5] and inorganic[6,7,8] acids have been reported. These examples share two common features: (1) a phase transition where the symmetry of the lattice changes from a high temperature paraelectric, non-polar, centrosymmetric space group, to a polar, non-centrosymmetric one below the phase transition temperature; (2) the polarizability of the ionic H-transfer complex is made possible by the strong acids[4,5] with pKa values comparable to or lower than that of $[H_2dabco]^{2+}$. An interesting possibility arises when one considers non-polar H-bonding complexes, i.e. weaker acids and dabco, that can adopt local polarization by breaking the symmetry of the H-bond, or by undergoing proton transfer reactions. We reasoned that it might be possible to take advantage of transient dipoles generated and synthesize materials

Scheme 1

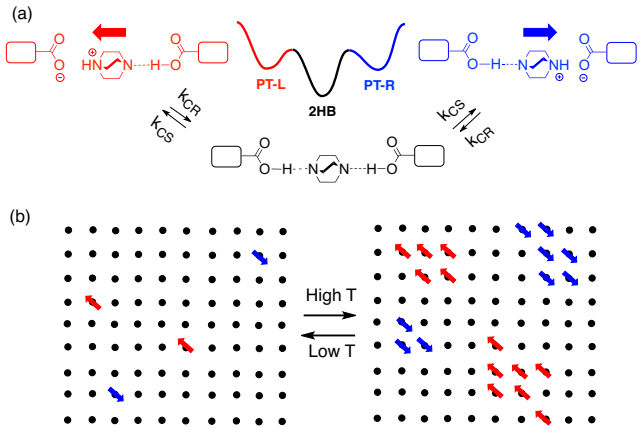

with a relatively large dielectric response and potentially transient ferroelectric behavior. As illustrated in Scheme 1, for a hypothetical model for a 2:1 complex with two neutral H-bonds (**2HB**) at the ground state, thermal activation of the ditopic structure would make it possible to access proton transferred states (**PT-L** and **PT-R**), providing a mechanism to

generate large charges that can change direction in response to local perturbations or external fields. Such thermally activated proton-transferred states, also known as *migrating protons*, have been previously reported in H-bonded systems.[9] We further propose that if properly aligned, correlation of transient, yet switchable dipoles lead to dipolar order in the nanoscale domain and relaxor-like behavior in the macroscale. In this paper, we report experimental temperature- and field-response results that support such a system. While changes in dipolar order could be documented by dielectric measurements, the lack of a phase transition was recognized by results from thermal analyses and the rotational dynamics of the highly symmetric dabco unit.

RESULTS AND DISCUSSION

Our initial design (Figure 1) was inspired by our experience in the study of crystalline molecular rotors[10] such as **1** and **2**. A 2:1 complex was expected for triphenylacetic acid **3** and dabco **5**, whereas the bidentate H-bond donor triptycene-9,10-dicarboxylic acid **4**[11] and dabco **5** would form infinite 1-D chains. Solvent-free cocrystals, that are indefinitely stable at ambient conditions, were obtained by layering a dabco solution in MeOH on top of a solution of acids **3** or **4** in a MeOH/DCM mixture followed by slow solvent evaporation. High quality single crystals obtained in this manner provided excellent diffraction data, which was solved with Rf values of 3.82% for **I** and 3.86% for **II**. The positions of the acidic hydrogen atoms involved in H-bonds were determined based on the electron density between the heavy atoms. The structure of the trityl carboxylic acid system **I** was solved in the space group P1-bar with the

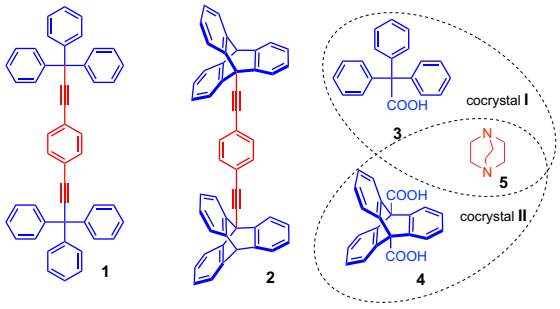

Figure 1. Molecular rotor **1** and **2**, and the supramolecular synthons **3**, **4**, and **5** for H-bonded molecular rotors.

unit cell of a trimeric complex formed by two molecules of **3** and one molecule of dabco **5**. The equilibrium structure of the complex is distorted from linearity and suggests that dabco is protonated on one side and hydrogen bonded on the other. The 2:1 complex packs in a slip-stack fashion similar to that observed with linear molecular rotors (Figure 2B). In the crystal, the protonated dabco resides in a pseudo 4-fold symmetric cavity formed by aromatic groups from surrounding triphenylacetate groups (Figure 2C). The mismatch between the intrinsic 3-fold symmetry of dabco and the 4-fold symmetric cavity suggest that dabco may occupy up to 12 nearly degenerate positions, which should result in a potential with relatively low rotational barriers. The crystal structure of complex **II** was also solved in the triclinic space group P1-bar with the repeating unit consisting of one molecule of triptycene dicarboxylate (TCD) **4**, and one molecule of dabco **5**. The expected 1D H-bond chains were indeed observed, each surrounded by 3 neighboring chains. Analysis of the packing environment shows that dabco resides in a cavity with a pseudo 3-fold symmetry (Figure 2F), which matches its own rotational symmetry, suggesting a relatively simple 3-fold rotational potential. Thermogravimetric analysis (TGA, supporting information, S4) showed that both crystal complexes are stable, with less than 1% weight loss observed below 446 K and 558 K, respectively, for **I** and **II**, and no phase transitions were observed in the differential scanning calorimeter.

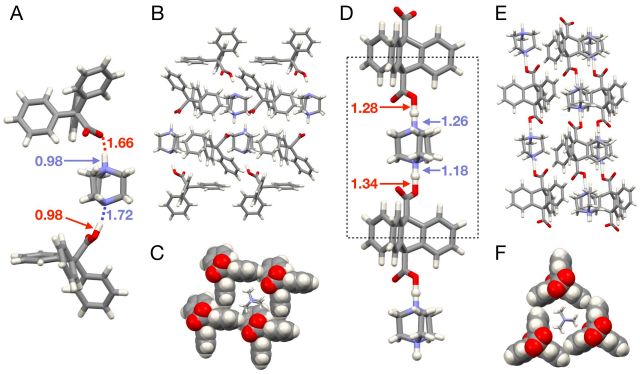

Figure 2. Crystal structures of cocrystals **I** and **II** showing (A) the unit cell, (B) the packing structure viewed along its *a* axis, and (C) the surrounding of dabco in the crystals in cocrystal **I**, (D) a chain of hydrogen bonds with two unit cells along the *c* axis, (E) the packing structure viewed along the *a* axis, and (F) the packing environment around dabco in cocrystal **II**. The dashed rectangle outlines one **2HB** unit depicted in Scheme 1.

The proton-transfer and neutral H-bonded sites in cocrystal **I** are characterized by typical N–H and O–H bonds that are 0.98 Å each, and H···O and H···N distances that are 1.66 and 1.72 Å, respectively. By contrast, the crystal structure cocrystal **II** is consistent with two neutral H-bonds in both directions of the chain. The X–H and H···Y distances are averaged in a X–H···Y H-bond while the distance between the heteroatoms is slightly shorter than that of a normal H-bond. The N–H and O–H bond are 1.18 and 1.28 Å, and H···O and H···N distances are 1.34 and 1.26 Å, respectively. Both H-bonds are almost linear (176 and 178°). Note that the position of H atoms described above is the equilibrium position, which is time averaged among configurations where H atoms are closer to either heavy atom.[9] A quick scan of the energy landscape of the outlined **2HB** unit in vacuum was performed by locking all atoms other than the two H atoms involved in the H-bonds. It was found that the O–H···N configuration is still favored over the equilibrium position in an isolated unit by 6-8 kcal/mol, an energy barrier that is comparable to the thermal energy.

Dielectric Measurements. To probe the postulated presence and/or generation of transient dipoles, as well as their response to external electric fields, we measured the dielectric response of polycrystalline samples of **I** and **II** with AC field frequencies varying between 100 and 10,000 Hz in the temperature range of 175 and 375 K (Figure 3 and SI). A priori, we expected the dielectric response from cocrystals **II** to arise from changes of the local dipoles as a result of charge separation. The real (ε') and imaginary (ε'') parts of the complex dielectric in the case of **I** showed no significant response, indicating that the sample cannot be polarized with the AC field frequen-

cies and temperatures explored in this study. This suggests that switching the site of proton transfer in complex **I** from one triphenylacetic acid group to the other must be energetically unfavorable. The corresponding data is included in the SI section.

By contrast, analogous measurements in the case of **II** (Figure 3) revealed an interesting dielectric response. The values of ε' in the case of **II** varied from ca. 26 to 35 with a non-symmetric signal that extends between ca. 200 K to 375 K and a peak value at ca. 298 K. The signal intensity is a function of the AC field frequency and increases from ca. 30 to 32 at the maximum with a baseline that starts at 26 and climbs up at ca. 28. The imaginary part of the dielectric (ε''), corresponding to the dielectric loss changes as a function of temperature, as shown in the bottom of Figure 3. Notably, the behavior of ε'' parallels the behavior of the dielectric constant, with (1) a very broad peak as a function of temperature, (2) no changes in the position of the maximum, and (3) a signal that increases with decreasing frequency between 10^5 Hz and 10^2 Hz.

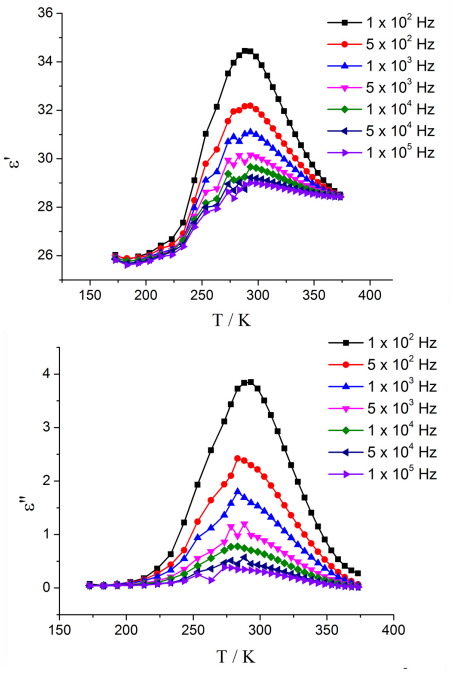

Figure 3. Temperature-dependence of (top) the real (ε') and (bottom) imaginary (ε'') parts of the complex dielectric for crystals **II** in the frequency range of 10^2 – 10^5 Hz.

If we consider the intensity of ε' in Figure 3a to be proportional to the number of dipoles that follow the AC field at the corresponding frequency and temperature, the results are consistent with the hypothesis depicted in Scheme 1. First of all, the equilibrium concentration of charges and their corresponding dipoles is a function of temperature and of the energy difference between the neutral complex (**2HB**) and the charge separated state (**PT-L** or **PT-R**). More interestingly, the response rate of the transient dipoles should be determined by the rates of charge separation (k_{CS}) and charge recombination (k_R) events. As suggested in the Scheme 1, dipolar switching will require (a) charge separation with a rate k_{CS} to generate a dipole in one direction, followed by (b) charge recombination with a rate k_R to form the neutral complex, and (c) a subsequent charge separation with a rate k_{CS} to generate a dipole in the opposite direction. Considering that the equilibrium concentration of dipoles and their rates of switching are expected to increase with temperature, one may speculate that the position of the maximum observed in the signal of ε' as a function of temperature and frequency is a manifestation of the local dipole order, which is likely to be paraelectric at high temperatures and potentially ferroelectric at and below the maximum. The fact that one does not observe changes in the ε'' maxima as a function of frequency, suggests that the dielectric behavior is limited by local order while the intensity of the signal is dependent by thermally controlled proton transfer dynamics. To explore these parameters, we turned our attention to solid-state NMR.

High Resolution Solid-State CPMAS ^{15}N NMR. As previously shown by Gobetto and coworkers,[12] the relatively large chemical shift dispersion of the ^{15}N nucleus and its high sensitivity to its electronic environment makes it a valuable probe to determine the protonation state of nitrogen in cocrystals formed between carboxylic acids and amines. Based on a correlation of single crystal X-ray diffraction and CPMAS ^{15}N NMR data, they showed that the chemical shifts of free amines, hydrogen bonded amines, and fully protonated quaternary ammonium nitrogen atoms are easily distinguishable with resonance frequencies ($^{15}NH_3$ at 0 ppm) of at ca. 12 ppm, 20 ppm, and 30 ppm, respectively. With that in mind, as shown in Figure 4, we carried out high resolution CPMAS ^{15}N NMR experiments with samples of cocrystals of **I** and **II**.

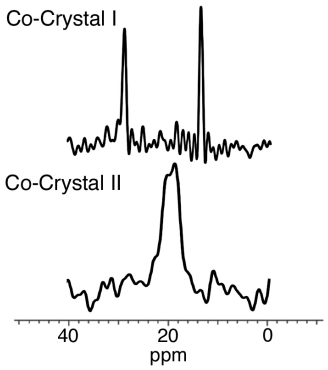

Figure 4. High resolution natural abundance CPMAS ^{15}N NMR experiments with samples of cocrystals of **I** and **II** showing evidence of neutral and proton transferred sites for dabco in **I**, and two hydrogen-bonded sites for dabco in **II**.

The spectra were recorded with natural abundance ^{15}N powdered samples spun at 10 kHz on an AV600 solid-state spectrometer utilizing 3.2 mm HXY CP/MAS probe at 60.82 MHz. A contact time of 5 ms and a delay of 25 s between pulses were used to acquire the ambient temperature spectra. The ^{15}N NMR chemical shifts were referenced using the resonance of solid glycine at 33.4 ppm. Temperature readings were calibrated with ^{207}Pb CPMAS NMR of $Pb(NO_3)_2$ at various temperatures.[13] The results obtained with cocrystal **I** revealed two signals separated by ca. 15 ppm, with

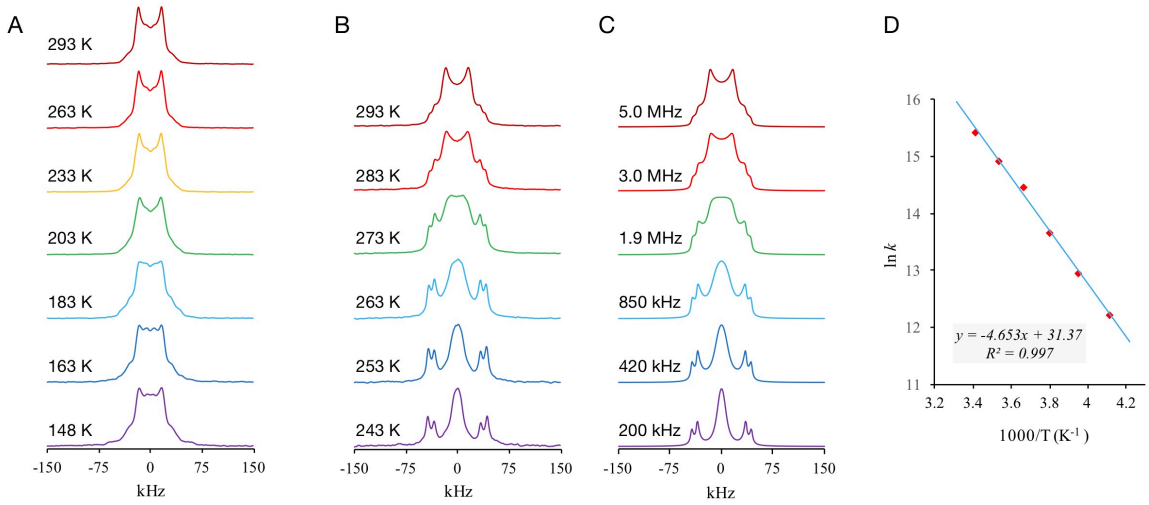

Figure 5. Experimental solid-state quadrupolar echo ^{2}H NMR spectra of (A) **I**-d_{12} and (B) **II**-d_{12}. (C) The simulated spectra of **II**-d_{12} and (D) corresponding Arrhenius plot where one can draw an activation energy for rotation of 9.2 kcal/mol and a pre-exponential factor of 4.2 × 10^{13} s^{-1} for dabco rotation in cocrystal **II**.

a neutral nitrogen signal at approximately 13.5 ppm and the quaternary ammonium signal at a lower field of 29 ppm (Figure 4, top). By contrast, cocrystal **II** displays two overlapping signals at ca. 19.5 and 18.0 ppm, which are in agreement with the single crystal stricture and is indicative of very two similar hydrogen bonding interactions present in the 1:1 infinite chain complex. A spectrum acquired at 386 K in the case of crystals **II** displayed no measurable change, suggesting that the concentration of charge separated species must be relatively small, which would also be consistent with a slow charge separation rate (k_{CS}) values.

Rotational Dynamics by ^{2}H NMR Line Shape Analysis. Our group has previously demonstrated that solid-state rotational dynamics can be highly sensitive to both physical and chemical changes in the solid phase.[14,15] We analyzed the dynamics of dabco in crystals of **I** and **II** in an effort to characterize changes in phase order of either system using line shape analysis of solid-state ^{2}H NMR spin-echo spectra.[16] It is well established that line shape analysis is a powerful method to determine the dynamics of crystalline solids in the frequency range that varies from ca. 10^4 to 10^7 Hz and based on our previous experience, we anticipated dabco rotation to occur in the megahertz regime for both complexes.

Cocrystals of **I**-d_{12} and **II**-d_{12} were prepared with dabco-d_{12} and their SS ^{2}H NMR spectra were obtained at a frequency of 46.07 MHz. The spectrum of **I**-d_{12} featured a relatively narrow spectrum of dabco at 293 K with two peaks separated by ca. 33 kHz, suggesting fast dynamics with a high symmetry potential (Figure 5A). When the sample is cooled to lower temperatures, two new peaks appeared at the center of the spectra. Further lowering the temperature to 148 K, the lowest possible temperature on our instrument, gave spectra with less pronounced central peaks but similar lineshape. Consequently, we could draw no conclusion other than dabco rotates faster than ca. 10^7 s^{-1} in complex **I**, even at the lowest temperatures measured.

In contrast, the SS ^{2}H NMR spectra of **II**-d_{12} were more complex, with a pronounced temperature dependence. As shown in Figure 5B, the 293 K spectrum resembles that of a 3-fold rotation at a relatively high rate (>10^6 s^{-1}). There are, however, some features at the shoulders that could not be reproduced by simulation with simple 3-fold or 6-fold rotational models. The same was true for spectra collected in the temperature range from 283 to 243 K, where the evolving side peaks split into doublets. Considering that dabco is desymmetrized due to differences in hydrogen bonding at the two nitrogen atoms, we reasoned that these doublets could be an indication of two QCCs[17] values. In fact, the experimental spectra were reproduced with a simple 3-fold rotation model with QCCs values of 110 and 135 kHz. The rate of rotation was estimated to be 5.0 MHz, 3.0 MHz, 1.9 MHz, 850 kHz, 420 kHz, and 200 kHz, at 293, 283, 273, 263, 253, and 243 K, respectively. Assuming dabco rotation is an elementary process to which the Arrhenius theory could be applied, we concluded that the activation energy for rotation is 9.2 kcal/mol with a pre-exponential factor of 4.2 × 10^{13} s^{-1} (Figure 5D). Unfortunately, being in the fast exchange regime at room temperature, the method is not amenable for the determination of discontinuities in the Arrhenius plot that may be indicative of an order-disorder phase transition.

Rotational Dynamics by ^{1}H NMR T_1 Spin-Lattice Relaxation. In a second attempt to detect potential changes in phase order using molecular rotation as a probe we decided to explore the use of solid-state ^{1}H NMR T_1 spin-lattice relaxation.[18] The method takes advantage of the modulation of dipolar coupling interactions at the Larmor frequency (ω_0) by rotational motion of a group that bears the nucleus of interest. Variation in the measured spin lattice relaxation values ($1/T_1$) as a function of temperature can be related to changes in the rotational correlation times, τ_c, as indicated by the Kubo-Tomita relaxation expression (Eq. 1),

$$T_1^{-1} = C\,[\tau_c(1 + \omega_0^2\,\tau_c^2)^{-1} + 4\tau_c(1 + 4\omega_0^2\,\tau_c^2)^{-1}] \qquad \text{Eq. 1}$$

where C is a constant related to the strength of the ^{1}H–^{1}H dipolar coupling and, assuming that rotation follows an Arrhenius behavior (Eq. 2), one can substitute the τ_c values in Eq. 1 with activation energy (E_a) and the pre-exponential factor for rotation (τ_0^{-1}) to characterize the dynamics of the dabco rotor.

$$\tau_c^{-1} = \tau_0^{-1}\exp(-E_a/RT) \qquad \text{Eq. 2}$$

The ^{1}H T_1 relaxation measurements were acquired with a saturation-recovery sequence at a Larmor frequency of 600.1 MHz for the samples of complexes **I** and **II**, as well as their deuterated analogs **I**-d_{12} and **II**-d_{12} (supporting information, S34)

The saturation-recovery kinetics of both **I** and **I**-d_{12} could be described well with a single exponential function, indicating that a single dynamic process is responsible for the relaxation of the sample. For complex **I**, relaxation rates ($1/T_1$) varied as shown in Figure 5 with a maximum at ca. 305 K and a fit to the Kubo−Tomita equation (Eq.1) suggesting an activation energy of 4.5 kcal/mol and a pre-exponential factor τ_0^{-1} of 1.8 × 10^{12} s^{-1}. These values match well with previously reported ^{1}H T_1 results for dabco in halogen bonded crystals,[Error! Bookmark not defined.] and are consistent with the ^{2}H NMR data in Figure 4A, showing that dabco undergoes fast rotation with site exchange rates that are ≈ 10^6 s^{-1} at temperatures as low as 163 K. It could be shown that dabco rotation is the relaxation mechanism when deuterated dabco in samples of **I**-d_{12} displayed ^{1}H T_1 values that are more than ten times longer than those of natural abundance **I**, consistent with the degree of deuteration of dabco of ca. 90%.

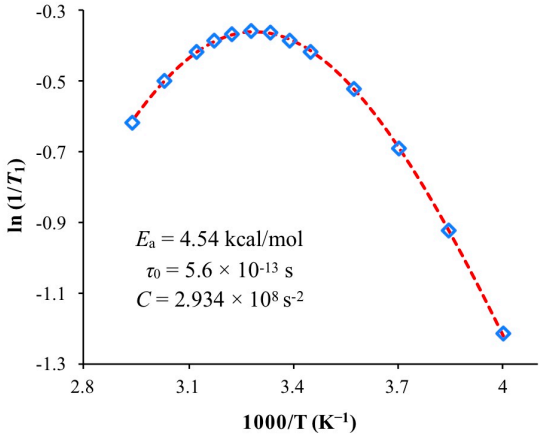

Figure 6. Temperature dependence of spin-lattice relaxation rate of **I**. Experimental data (blue squares) was fitted (red dashed curve) to Kubo−Tomita equation to obtain energetic parameters of the dynamic process.

In the case of crystalline supramolecular rotor **II**, ^{1}H T_1 measurements revealed kinetics with a long-lived component, that accounts for 98-99% of the total intensity, varying from 36.6 s at 300 K to 4.8 s at 370 K (Table 1). Notably, a systematic decrease in the T_1 values as a function of increasing temperature suggest that the frequency of the dynamic process responsible for relaxation approaches the Larmor frequency (600.1 MHz) as the temperature is higher.

Once again, the process that is responsible for the observed relaxation is rotation of the dabco group could be confirmed by ^{1}H T_1 measurements of isotopically labeled **II**-d_{12}, which displayed very long and complex relaxation kinetics. A plot of the Ln T_1 vs 1/T from natural abundance **II** is expected to have a slope that corresponding to Ea/R, which gives an activation of ca. 8 ± 2 kcal/mol, and is consistent with the results from ^{2}H NMR line shape analysis (Figure 4). Notably, the corresponding Arrhenius plot does not show a discontinuity at ca. 298 K, confirming the absence of first-order transitions, and the limited domain size of structural features responsible for the dielectric signals.

Table 1. Summary of the T_1 data of II, and II-d_{12}.

Sample	T/K	T_1/s (weighted contribution, %[a])
II	300	36.6 (*99*), 1.2 (*1*)
II	310	28.6 (*99*), 1.2 (*1*)
II	320	21.2 (*99*), 1.1 (*1*)
II	330	15.6 (*99*), 1.0 (*1*)
II	340	11.5 (*98*), 1.0 (*2*)
II	350	8.4 (*98*), 0.87 (*2*)
II	370	4.8 (*98*), 0.61 (*2*)
II-d_{12}	300	500.1 (*42.8*), 100.0 (*39.4*), 1.7 (*17.8*)
II-d_{12}	320	285.8 (*51.3*), 72.5 (*31.7*), 1.6 (*17.1*)
II-d_{12}	350	115.0 (*72.5*), 19.1 (*13.1*), 1.3 (*14.2*)

[a]The weighted contribution for component *i*, was obtained with the formula $\%(i) = I_i T_{1i} / \sum I_i T_{1i}$

Variable Temperature X-Ray Diffraction Measurements

The last experimental test to probe changes in proton transferred equilibrium and or/phase transitions was based on VT single crystal XRD of cocrystals **I** and **II**. In addition to the original 100 K data, diffraction data was collected at 200 and 300 K for **I**, and 300 and 350 K for **II** (Figure 7).

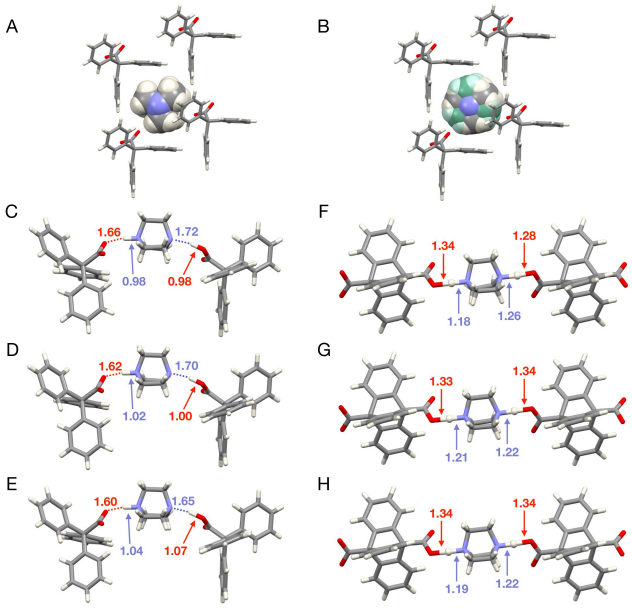

Figure 7. Variable temperature XRD structures showing differences between the low temp and high temp structure of **I** and **II**. (A, B) Space-filling model of showing the positional disorder of dabco (6%, shown in green) occupying a new position at 300 K. The distance between H and heteroatoms in the hydrogen bonds of **I** at 100 (C), 200 (D), and 300 K (E); of **II** at 100 (F), 300 (G), and 350 K (H).

No observable phase transition/symmetry breaking was observed in either structure. A 6% positional disorder of dabco in **I** was observed at 300 K, suggesting an asymmetrical 6-fold rotational potential, which is in good agreement with the symmetry mismatch of dabco (3-fold) and the cavity (4-fold)

where it resides. Such disorder was not observed for **II**, confirming the 3-fold rotational potential suggested by SS ^{2}H NMR experiments.

We next focused on the temperature dependence of H-bond parameters. For complex **I**, the O–H distance in the normal H-bond increases from 0.98 Å (100 K) to 1.00 Å (200 K) and 1.07 Å (300 K). Corresponding changes in the H···N bond include a decrease in distance from 1.72 to 1.70 to 1.65 Å at the corresponding temperatures. The distance between O and N remains the same. Similarly, on the other end of dabco, where proton-transferred occurs, the N–H distance increases and H···O distance decreases with temperature. The changes are less significant for complex **II** as the hydrogen atoms are located much closer to the middle of two heteroatoms to begin with. The only feature worth noticing was that at 300 and 350 K, both hydrogen atoms in the hydrogen bonds are rather close to the nitrogen atom, rendering the overall equilibrium structure reminiscent of a complex where two sides are able to explore proton-transferred states.[9]

CONCLUSIONS

Cocrystals formed with dabco and either tritylcarboxylic acid **3** (cocrystal **I**) or triptycene-9,10-dicarboxylate **4** (cocrystal **II**) were shown to display charge transfer and neutral hydrogen bonding interactions that were documented by single crystal X-ray diffraction and solid-state CPMAS ^{15}N NMR. While low frequency measurements of the real and imaginary part of the complex dielectric carried between 150 K and 400 K in the case of complex **I** reveal no significant response, cocrystal **II** showed a very broad peak with a maximum at ca. 275 K. The dielectric signals were characterized by having a peak maximum with a position that is independent of both temperature and AC field frequencies, although the size of the signal was shown to increase from 10^{5} to 10^{2} Hz. Rotational dynamics measurements in the solid state carried out using quadrupolar echo ^{2}H NMR and ^{1}H NMR spin lattice relaxation measurements revealed fast rotational motion but no indications of a phase transition or structural changes that could help account for the dielectric behavior. We interpret the dielectric data in terms of a model that requires thermally activated proton transfer events to generate and switch the dipoles responsible for the sample polarization. The fact that there are no changes in the crystal structure and the lack of proton transferred signals in the ^{15}N NMR suggests that the charge transfer dipoles are transient and occur at a very low concentration, perhaps localized within very small domains. The characteristics of the dielectric peak can be interpreted in terms of a paraelectric state at high temperature that changes to one where the dipoles are ordered, potentially in a ferroelectric state below the maximum at lower temperatures. Finally, an increase in the intensity of the signal as a function of decreasing AC field frequency is consistent with a process that occurs with a relatively high barrier, as it would be expected from the proton transfer in cocrystal **I**. Further dielectric and polarization measurements with cocrystals **I** and **II** and substituted analogs will help shed light on this interesting behavior.

ASSOCIATED CONTENT

Supporting Information

Single crystal structures for co-crystals I and II have been deposited, respectively, as CCDC 1938953-1938958. Sample preparation, instruments, and sample characterization (pdf). This material is available free of charge via the Internet at http://pubs.acs.org.

AUTHOR INFORMATION

Corresponding Author

*mgg@chem.ucla.edu

*duanhaibao4660@163.com

Funding Sources

This work was supported by National Science Foundation grants DMR 1700471 (M.A.G.-G.) and MRI 1532232, and by Nature Science Foundation of JiangSu Province (BK20171125, H.-B.D).

ACKNOWLEDGMENT

We thank Mr. Yun Jia for help with T_1 data analysis and Dr. Zhikun Cai and Dr. Jianxiao Gong for helpful discussions.

REFERENCES

1 (a) Atwood, J. L.; Gokel, G. W.; Barbour, L. Eds. Comprehensive Supramolecular Chemistry II; Oxford: Elsevier. Vol. 7, pp. 25–48. ISBN: 9780128031988. (b) Braga, D,; Maini, L.; Polito, M.; Greponi, F. Hydrogen Bonding Interactions Between Ions: A Powerful Tool in Molecular Crystal Engineering. *Structure and Bonding* **2004**, *111*, 1–32.

2 (a) Sato, O. Dynamic Molecular Crystals with Switchable Physical Properties. *Nat. Chem.* **2016**, *8*, 644–656. (b) Tayi, A. S.; Kaeser, A.; Matsumoto, M.; Aida, T.; Stupp, S. I. Supramolecular Ferroelectrics. *Nat. Chem.* **2015**, *7*, 281–294. (c) Fu, D.-W.; Cai, H.-L.; Liu, Y.; Ye, Q.; Zhang, W.; Zhang, Y.; Chen, X.-Y.; Giovannetti, G.; Capone, M.; Li, J.; Xiong, R.-G. Diisopropylammonium Bromide Is a High-Temperature Molecular Ferroelectric Crystal. *Science* **2013**, *339*, 425–428. (d) Akutagawa, T.; Koshinaka, H.; Sato, D.; Takeda, S.; Noro, S.-I.; Takahashi, H.; Kumai, R.; Tokura, Y.; Nakamura, T. Ferroelectricity and Polarity Control in Solid-State Flip-Flop Supramolecular Rotators. *Nat. Mater.* **2009**, *8*, 342–347. (e) Horiuchi, S.; Tokura, Y. Organic Ferroelectrics. *Nat. Mater.* **2008**, *7*, 357–366. (f) Horiuchi, S.; Ishii, F.; Kumai, R.; Okimoto, Y.; Tachibana, H.; Nagaosa, N.; Tokura, Y. Ferroelectricity near Room Temperature in Co-Crystals of Nonpolar Organic Molecules. *Nat. Mater.* **2005**, *4*, 163–166.

3 Benoit, R. L.; Lefebvre, D.; Fréchette, M. Basicity of 1,8-Bis(dimethylamino)naphthalene and 1,4-Diazabicyclo[2.2.2]octane in Water and Dimethylsulfoxide. *Can. J. Chem.* **1987**, *65*, 996–1001.

4 Yao, Z.-S.; Yamamoto, K.; Cai, H.-L.; Takahashi, K.; Sato, O. Above Room Temperature Organic Ferroelectrics: Diprotonated 1,4-Diazabicyclo[2.2.2]octane Shifts between Two 2-Chlorobenzoates. *J. Am. Chem. Soc.* **2016**, *138*, 12005–12008.

5 Akutagawa, T.; Takeda, S.; Hasegawa, T.; Nakamura, T. Proton Transfer and a Dielectric Phase Transition in the Molecular Conductor $(HDABCO^{+})_2(TCNQ)_3$. *J. Am. Chem. Soc.* **2007**, *126*, 291–294.

6 (a) Szafranski, M.; Katrusiak, A.; McIntyre, G. J. Ferroelectric Order of Parallel Bistable Hydrogen Bonds. *Phys. Rev. Lett.* **2002**, *89*, 215507. (b) Katrusiak, A.; Szafranski, M. Ferroelectricity in NH···N Hydrogen Bonded Crystals. *Phys. Rev. Lett.* **1999**, *82*, 576–579. (c) Szafrański, M.; Katrusiak, A. Short-Range Ferroelectric Order Induced by Proton Transfer-Mediated Ionicity. *J. Phys. Chem. B* **2004**, *108*, 15709–15713.

7 Chen, C.; Zhang, W.-Y.; Ye, H.Y.; Fu, D.-W. Rapid Dielectric Bistable Switching Materials Without a Time/temperature Responsive Blind Area in the Linarite-like Type Molecular Large-size Single Crystals. *J. Mat. Chem. C.* **2016**, *4*, 9009–9020.

8 Zhang, Y.; Zhang, W.; Li, S.-H.; Ye, Q.; Cai, H.-L.; Deng, F.; Xiong, R.-G. Huang, S. D. Ferroelectricity Induced by Ordering of

Twisting Motion in a Molecular Rotor. *J. Am. Chem. Soc.* **2012**, *134*, 11044–11049.

9 (a) Steiner, T.; Majerz, I.; Wilson, C. C. First O−H−N Hydrogen Bond with a Centered Proton Obtained by Thermally Induced Proton Migration. *Angew. Chem. Int. Ed.* **2001**, *40*, 2651–2654. (b) Coles, M. P.; Khalaf M. S.; Claramunt, R. M.; García, M. A.; Alkorta, I.; Elguero, J. Double Proton Transfer in Crystals of 1,3,4,6,7,8-Hexahydro-2H-pyrimido[1,2-a] Pyrimidine (hppH): ^{13}C and ^{15}N CPMAS NMR study of $(hppH)_2$. *J. Phys. Org. Chem.* **2010**, *23*, 526–535. (c) Jones A. O. F.; Blagden, N.; McIntyre, G. J.; Parkin, A.; Seaton, C. C.; Thomas, L. H.; Wilson, C. C. Tuning Proton Disorder in 3,5-Dinitrobenzoic Acid Dimers: the Effect of Local Environment. *Cryst. Growth Des.* **2013**, *13*, 497–509. (d) Majerz, I.; Gutmann, M. J. Intermolecular OHN Hydrogen Bond with a Proton Moving in 3-Methylpyridinium 2,6-Dichloro-4-nitrophenolate. *RSC Adv.* **2015**, *5*, 95576–95584. (e) Guo, J.; Tolstoy, P. M.; Koeppe, B.; Denisov G. S.; Limbach, H.-H. NMR Study of Conformational Exchange and Double-Well Proton Potential in Intramolecular Hydrogen Bonds in Monoanions of Succinic Acid and Derivatives. *J. Phys. Chem. A* **2011**, *115*, 9828–9836.

10 For selected examples of solid-state molecular rotors, see (a) Kaleta, J.; Bastien, G.; Wen, J.; Dračínský, M.; Tortorici, E.; Císařová, I.; Beale, P. D.; Rogers, C. T.; Michl, J. Bulk Inclusions of Double Pyridazine Molecular Rotors in Hexagonal Tris(o-phenylene) cyclotriphosphazene. *J. Org. Chem.* **2019**, *84*, 8449-8467. (b) Zhu, K.; Baggi, G.; Loeb, S. J. Ring-through-Ring Molecular Shuttling in a Saturated [3]Rotaxane. *Nat. Chem.* **2018**, *10*, 625–630. (c) Tsurunaga, M.; Inagaki, Y.; Momma, H.; Kwon, E.; Yamaguchi, K.; Yoza, K.; Setaka, W. Dielectric Relaxation of Powdered Molecular Gyrotops Having a Thiophene Dioxide-Diyl as a Dipolar Rotor. *Org. Lett.* **2018**, *20*, 6934–6937. (d) Bracco, S.; Castiglioni, F.; Comotti, A.; Galli, S.; Negroni, M.; Maspero, A.; Sozzani, P. Ultrafast Molecular Rotors and Their CO_2 Tuning in MOFs with Rod-Like Ligands. *Chem. Eur. J.* **2017**, *23*, 11210–11215. (e) Jiang, X.; O'Brien, Z. J.; Yang, S.; Lai, L. H.; Buenaflor, J.; Tan, C.; Khan, S.; Houk, K. N.; Garcia-Garibay, M. A. Crystal Fluidity Reflected by Fast Rotational Motion at the Core, Branches, and Peripheral Aromatic Groups of a Dendrimeric Molecular Rotor. *J. Am. Chem. Soc.* **2016**, *138*, 4650–4656. (f) Lemouchi, C.; Iliopoulos, K.; Zorina, L.; Simonov, S.; Wzietek, P.; Cauchy, T.; Rodríguez-Fortea, A.; Canadell, E.; Kaleta, J.; Michl, J.; Gindre, D.; Chrysos, M.; Batail, P. Crystalline Arrays of Pairs of Molecular Rotors: Correlated Motion, Rotational Barriers, and Space-Inversion Symmetry Breaking Due to Conformational Mutations. *J. Am. Chem. Soc.* **2013**, *135*, 9366–9376. (g) Akutagawa, T.; Endo, D.; Kudo, F.; Noro, S.; Takeda, S.; Cronin, L.; Nakamura, T. A Solid-State Supramolecular Rotator Assembled from a Cs-crown Ether Polyoxometalate Hybrid: $(Cs^+)_3([18]crown\text{-}6)_3(H^+)_2[PMo_{12}O_{40}]$. *Cryst. Growth Des.* **2008**, *3*, 812–816.

11 Klanderman, B. H.; Faber, J. W. H. Novel Bridged Anthracene Derivatives and Polyesters and Copolyesters Therefrom. *J. Polym. Sci., Part A1* **1968**, *6*, 2955–2965.

12 (a) Gobetto, R.; Nervi, C.; Valfrè, E.; Chierotti, M. R.; Braga, D.; Maini, L.; Grepioni, F.; Harris, R. K.; Ghi, P. Y. ^1H MAS, ^{15}N CPMAS, and DFT Investigation of Hydrogen-Bonded Supramolecular Adducts between the Diamine 1,4-Diazabicyclo-[2.2.2]octane and Dicarboxylic Acids of Variable Chain Length. *Chem. Mater.* **2005**, *17*, 1457. (b) Braga, D.; Maini, L.; de Sanctis, G.; Rubini, K.; Grepioni, F.; Chierotti, M. R.; Gobetto, R. Mechanochemical Preparation of Hydrogen-Bonded Adducts Between the Diamine 1,4-Diazabicyclo[2.2.2]octane and Dicarboxylic Acids of Variable Chain Length: An X-ray Diffraction and Solid-State NMR Study. *Chem. Eur. J.* **2003**, *9*, 5538–5548.

13 Bielecki, A.; Burum, D. P. Temperature Dependence of ^{207}Pb MAS Spectra of Solid Lead Nitrate. An Accurate, Sensitive Thermometer for Variable-Temperature MAS. *J. Magn. Reson.* **1995**, *116*, 215-220.

14 Catalano, L.; Perez-Estrada, S.; Metrangolo, P.; Wang, S. H.; Ayitou, A. J.-L. Brown, S.; Garcia-Garibay, M. A. Rotational Dynamics of Diazabicyclo[2.2.2]octane in Isomorphous Halogen-Bonded Co-crystals: Entropic and Enthalpic Effects. *J. Am. Chem. Soc.* **2017**, *139*, 843–848.

15 Simonov S.; Zorina, L.; Wzietek, P. Rodríguez-Fortea, A.; Canadell, E.; Mézière, C.; Bastien, G.; Lemouchi, C.; Garcia-Garibay, M. A. Batail, P. Static Modulation Wave of Arrays of Halogen Interactions Transduced to a Hierarchy of Nanoscale Change Stimuli of Crystalline Rotors Dynamics. *Nano Lett.*, **2018**, *18*, 3780–3784.

16 (a) Hansen, M. R.; Graf, R.; Spiess, H. W. Solid-State NMR in Macromolecular Systems: Insights on How Molecular Entities Move. *Acc. Chem. Res.* **2013**, *46*, 1996–2007. (b) Macho, V.; Brombacher, L.; Spiess, H. W. The NMR-WEBLAB: An Internet Approach to NMR Lineshape Analysis. *Appl. Magn. Reson.* **2001**, *20*, 405–432.

17 Khudozhitkov, A. E.; Stange, P.; Golub, B.; Paschek, D.; Stepanov, A. G.; Kolokolov, D. I.; Ludwig, R. Characterization of Doubly Ionic Hydrogen Bonds in Protic Ionic Liquids by NMR Deuteron Quadrupole Coupling Constants: Differences to H-Bonds in Amides, Peptides, and Proteins. *Angew. Chem. Int. Ed.* **2017**, *56*, 14310–14314.

18 (a) Beckmann, P. A.; Mallory, C. W.; Mallory, F. B.; Rheingold, A. L.; Wang, X. Methoxy and Methyl Group Rotation: Solid-State NMR ^1H Spin-Lattice Relaxation, Electronic Structure Calculations, X-ray Diffractometry, and Scanning Electron Microscopy. *ChemPhysChem* **2015**, *16*, 1509–1519. (b) Rodríguez-Molina, B.; Pérez-Estrada, S.; Garcia-Garibay, M. A. Amphidynamic Crystals of a Steroidal Bicyclo[2.2.2]octane Rotor: A High Symmetry Group That Rotates Faster than Smaller Methyl and Methoxy Groups. *J. Am. Chem. Soc.* **2013**, *135*, 10388–10395.

Table of contents graphic